Biochemical and Biophysical Research Communications 455 (2014) 332–338

Contents lists available at ScienceDirect

Biochemical and Biophysical Research Communications

journal homepage: www.elsevier.com/locate/ybbrc

Treatment with insulin-like growth factor 1 receptor inhibitor reverses hypoxia-induced epithelial–mesenchymal transition in non-small cell lung cancer

Fariz Nurwidya [a,b,1], Fumiyuki Takahashi [a,b,*,1], Isao Kobayashi [a,b], Akiko Murakami [a,b], Motoyasu Kato [a,b], Kunihiko Minakata [a,b], Takeshi Nara [c], Muneaki Hashimoto [c], Shigehiro Yagishita [a,b], Hario Baskoro [a,b], Moulid Hidayat [a,b], Naoko Shimada [a,b], Kazuhisa Takahashi [a,b]

[a] Department of Respiratory Medicine, Juntendo University Graduate School of Medicine, Tokyo, Japan
[b] Research Institute for Diseases of Old Ages, Juntendo University Graduate School of Medicine, Tokyo, Japan
[c] Department of Molecular and Cellular Parasitology, Juntendo University Graduate School of Medicine, Tokyo, Japan

ARTICLE INFO

Article history:
Received 27 October 2014
Available online 15 November 2014

Keywords:
IGF1R signaling
EMT
NSCLC

ABSTRACT

Insulin-like growth factor 1 receptor (IGF1R) is expressed in many types of solid tumors including non-small cell lung cancer (NSCLC), and enhanced activation of IGF1R is thought to reflect cancer progression. Epithelial–mesenchymal transition (EMT) has been established as one of the mechanisms responsible for cancer progression and metastasis, and microenvironment conditions, such as hypoxia, have been shown to induce EMT. The purposes of this study were to address the role of IGF1R activation in hypoxia-induced EMT in NSCLC and to determine whether inhibition of IGF1R might reverse hypoxia-induced EMT. Human NSCLC cell lines A549 and HCC2935 were exposed to hypoxia to investigate the expression of EMT-related genes and phenotypes. Gene expression analysis was performed by quantitative real-time PCR and cell phenotypes were studied by morphology assessment, scratch wound assay, and immunofluorescence. Hypoxia-exposed cells exhibited a spindle-shaped morphology with increased cell motility reminiscent of EMT, and demonstrated the loss of E-cadherin and increased expression of fibronectin and vimentin. Hypoxia also led to increased expression of IGF1, IGF binding protein-3 (IGFBP3), and IGF1R, but not transforming growth factor β1 (TGFβ1). Inhibition of hypoxia-inducible factor 1α (HIF1α) with YC-1 abrogated activation of IGF1R, and reduced IGF1 and IGFBP3 expression in hypoxic cells. Furthermore, inhibition of IGF1R using AEW541 in hypoxic condition restored E-cadherin expression, and reduced expression of fibronectin and vimentin. Finally, IGF1 stimulation of normoxic cells induced EMT. Our findings indicated that hypoxia induced EMT in NSCLC cells through activation of IGF1R, and that IGF1R inhibition reversed these phenomena. These results suggest a potential role for targeting IGF1R in the prevention of hypoxia-induced cancer progression and metastasis mediated by EMT.

1. Introduction

Insulin-like growth factor 1 receptor (IGF1R) is a transmembrane receptor tyrosine kinase, and is expressed in many types of cancer cells, including non-small cell lung cancer (NSCLC) [1]. IGF1R is activated by binding of its ligand, IGF1, leading to phosphorylation of phosphatidylinositol 3-kinase (PI3K) and phospholipase C gamma (PLCγ) that produces inositol 1,4,5-trisphosphate (IP_3) followed by Ca^{2+} release [2]. Cell signaling via IGF1R is essential in a variety of cellular processes including cancer progression [1].

Advanced NSCLC is the leading cause of cancer-related deaths worldwide [3]. Drug-resistance, metastasis, and invasion are some of the features of fatal cancer, and accumulating evidence has shown that metastasis and invasion are associated with an epithelial–mesenchymal transition (EMT) [4,5].

EMT is characterized by the dissolution of cell–cell junctions and loss of apico-basolateral polarity, resulting in the formation of migratory mesenchymal cells with invasive properties [6]. During

Abbreviations: DAPI, 4′,6-diamidino-2-phenylindole; YC-1, 5-[1-(phenylmethyl)-1H-indazol-3-yl]-2-furanmethanol; IGF1R, insulin-like growth factor 1 receptor; IGFBP3, insulin-like growth factor-binding protein 3; phospho-IGF1R, phospho-insulin-like growth factor 1; HIF1α, hypoxia-inducible factor 1α; DMSO, dimethyl sulfoxide; qPCR, quantitative real-time PCR.

* Corresponding author at: Department of Respiratory Medicine, Juntendo University, Graduate School of Medicine, 2-1-1 Hongo, Bunkyo-Ku, Tokyo 113-8421, Japan. Fax: +81 3 5802 1617.
E-mail address: fumiyuki@dol.hi-ho.ne.jp (F. Takahashi).

[1] These authors contributed equally to this study.

http://dx.doi.org/10.1016/j.bbrc.2014.11.014
0006-291X/

EMT, cells loose expression of the epithelial marker E-cadherin, and gain the mesenchymal markers vimentin and fibronectin. The mesenchymal state is associated with the capacity of cells to migrate to distant organs during the initiation of metastasis [7]. Several factors have been found to be capable of inducing EMT, including transforming growth factor β (TGFβ) [8] and tumor necrosis factor α (TNFα) [9]. Solid tumors often contain regions with insufficient oxygen delivery, a condition known as hypoxia, and several recent reports have suggested that hypoxia might also induce EMT [10]. Hypoxia-induced EMT has been investigated in various cancers, including gastric cancer [11], hepatocellular [12] and renal cell carcinomas [13]. The stabilization of hypoxia-inducible factor 1α (HIF-1α) by hypoxia allows for activation of EMT-inducer. It has been reported that under hypoxic conditions, pancreatic carcinoma cells lost cell–cell adhesion due to down-regulation of E-cadherin and concomitant up-regulation of vimentin [14]. In another study, hypoxic stress induced EMT in colon cancer cells, through β1-integrins and chemokine receptor type 4 (CXCR4) [15].

It has been reported that IGF1R is implicated in EMT-mediated invasiveness in gastric cancer [16]. However, a direct linkage of IGF1R activation with hypoxia and EMT has not been clarified. In the present study, we aimed to investigate whether activation of IGF1R is involved in hypoxia-induced EMT in NSCLC cells and to elucidate whether inhibition of IGF1R could reverse such hypoxia-induced EMT.

2. Materials and methods

2.1. Cell culture and reagents

NSCLC cell lines, A549 and HCC2935, were purchased from the American Type Culture Collection (Rockville, MD, USA). HCC2935 cells were cultured in RPMI-1640 medium (Wako Pure Chemical Industries, Osaka, Japan), while A549 was maintained in DMEM medium (Invitrogen, Carlsbad, CA, USA); both media were supplemented with 10% fetal bovine serum (FBS), 100 U/mL penicillin and 100 μg/mL streptomycin. Cell lines were verified to be mycoplasma-free using the MycoAlert Kit (Lonza, Amagazaki, Japan). Cells were grown in a humidified 5% CO_2 atmosphere at 37 °C in an incubator, in which the oxygen tension was held at either 21% (normoxia) or 1% (hypoxia). AEW541 was purchased from Selleck Chemicals (Houston, TX, USA) and YC-1 was purchased from Sigma–Aldrich (St. Louis, MO, USA).

2.2. Morphological analysis

Cells were visualized at 200× magnification with an Olympus light microscope (Olympus, Tokyo, Japan). Digital images of the A549 and HCC2935, in both normoxic and hypoxic conditions were randomly captured and examined for morphologic characteristics consistent with EMT. Spindle-shaped cells were counted and divided by the total cell number from each image to obtain the spindle-shaped cell percentage. Results were displayed as the means of spindle-shaped cell percentages from 5 images.

2.3. Wound healing scratch assay

A549 and HCC2935 cells were seeded in 6-well plate and allowed to attach to the plate surface for 24 h. A scratch was made in the center of the culture well using a sterile 200-μL micropipette tip and images were captured immediately after the scratch at 0 h and again after 24 h incubation at 37 °C in both normoxia and hypoxic conditions.

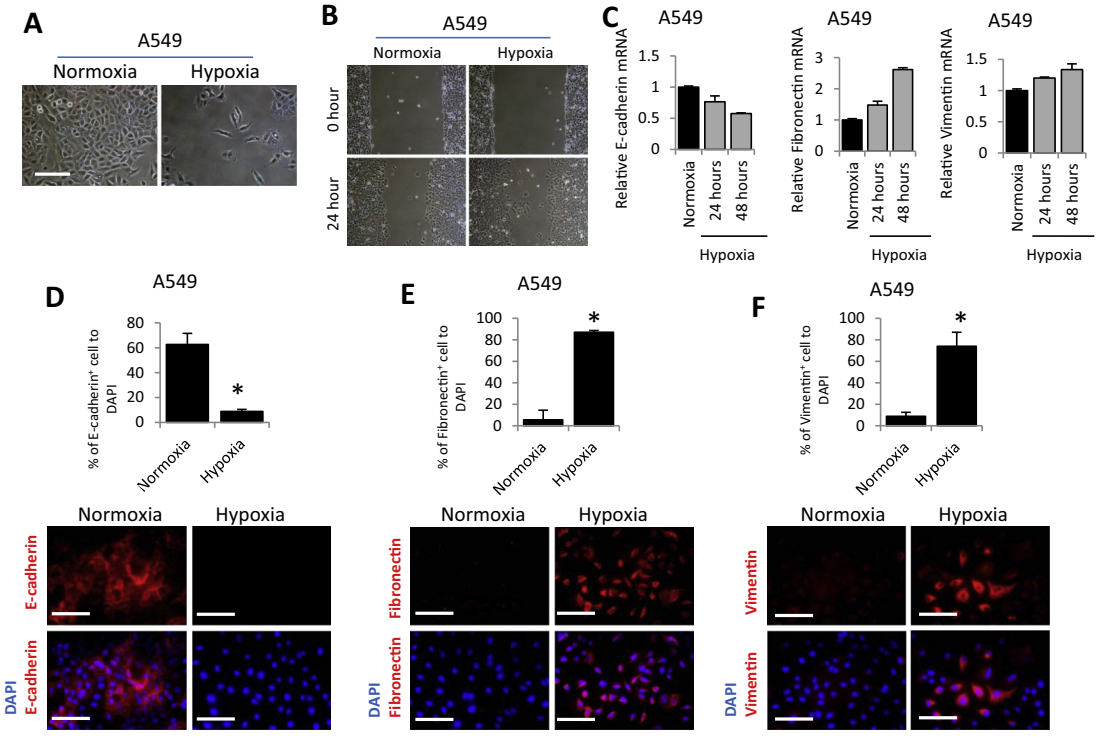

Fig. 1. Hypoxia induced EMT in A549 cells. (A) Hypoxia altered cell morphology to irregular and spindle-shaped. (B) Scratch was generated in the center of the culture well at 0 and after 24 h in normoxic or hypoxic conditions. (C) Quantitative real-time PCR was performed with primers specific for E-cadherin, fibronectin, and vimentin in A549 parental and hypoxic cells (24 and 48 h), and data were normalized to actin expression. (D–F) A549 cells, grown on Lab-Tek chamber slides, were exposed to normoxia or hypoxia for 24 h, fixed, and incubated with primary antibodies against E-cadherin (D), fibronectin (E), or vimentin (F) followed by secondary antibodies labeled with Alexa Fluor 488 anti-rabbit IgG (red). Cell nuclei were stained with DAPI (blue). Images were obtained using Axioplan 2 system. Five images were captured from each group and E-cadherin$^+$, vimentin$^+$, and fibronectin$^+$ cells numbers were divided by the corresponding DAPI numbers. Data are expressed as the means ± standard deviation. $^*P < 0.05$ indicates a significant difference from control group. Scale bar indicates 200 μM. (For interpretation of the references to color in this figure legend, the reader is referred to the web version of this article.)

2.4. Quantitative real-time PCR (qPCR)

Total RNA was extracted from cell lines using miRvana miRNA Isolation kit (Ambion, Austin, TX, USA) according to the manufacturer's instructions. Five hundred nanograms of total RNA was reverse-transcribed to cDNA using Revertra cDNA synthesis kit (Toyobo, Osaka, Japan). qPCR was performed using SYBR Green Master Mix (Toyobo). Cycling conditions were as follows: denaturation hold at 95 °C for 20 s, 40 cycles amplification (denaturation at 95 °C for 3 s, annealing and extension at 60 °C for 30 s), and melting-curve analysis. qPCR was performed in triplicate and expression levels of β-actin were used as internal controls. The primers that were specific for the genes were as follows:

Fibronectin
Forward, 5′-GAAGCCGAGGTTTTAACTGC-3′
Reverse, 5′-ACCCACTCGGTAAGTGTTCC-3′
Vimentin
Forward, 5′-AATTGCAGGAGGAGATGCTT-3′
Reverse, 5′-GAGACGCATTGTCAACATCC-3′
E-cadherin
Forward, 5′-CACGGTAACCGATCAGAATG-3′
Reverse, 5′-ACCTCCATCACAGAGGTTCC-3′
IGF1
Forward, 5′-GCTCTTCAGTTCGTGTGTGGA-3′
Reverse, 5′-CGACTGCTGGAGCCATACC-3′
IGFBP3
Forward, 5′-AGAGCACAGATACCCAGAACT-3′
Reverse, 5′-TGAGGAACTTCAGGTGATTCAGT-3′
IGF1R
Forward, 5′-CCATTCTCATGCCTTGGTCT-3′
Reverse, 5′-TGCAAGTTCTGGTTGTCGAG-3′
Actin
Forward, 5′-CTCTTCCAGCCTTCCTTCCT-3′
Reverse, 5′-AGCACTGTGTTGGCGTACAG-3′

2.5. Immunofluorescence

A549 and HCC2935 cells were seeded on Lab-Tek chamber II slides (Nunc, Rochester, NY, USA) under normoxia or hypoxia for 24 h, fixed with 8% paraformaldehyde for 20 min, and permeabilized with 0.1% Triton® X-100 for 3 min. After blocking with 10% goat serum in PBS for 30 min at room temperature, cells were incubated at 4 °C overnight with primary antibodies, followed by incubation with secondary antibody labeled with Alexa Fluor® 488 goat anti-rabbit IgG or Alexa Fluor® 594 goat anti-mouse IgG (Invitrogen, Carlsbad, CA, USA). Slides were mounted with Vectashield Mounting Medium with DAPI (Vector Laboratories, Burlingame, CA, USA). Images were captured on an Axioplan-2 imaging system (ZEISS, Oberkochen, Germany) with AxioVision software (ZEISS). Images used for comparisons of different cells and/or treatments were acquired with the same instrument settings and exposure times and were processed equivalently. The percentage of E-cadherin$^+$, vimentin$^+$, fibronectin$^+$, IGF1$^+$, IGF binding protein 3 (IGFBP3)$^+$, and phopho-IGF1R$^+$ cells to DAPI were calculated in every captured field, and mean was obtained from five fields. We

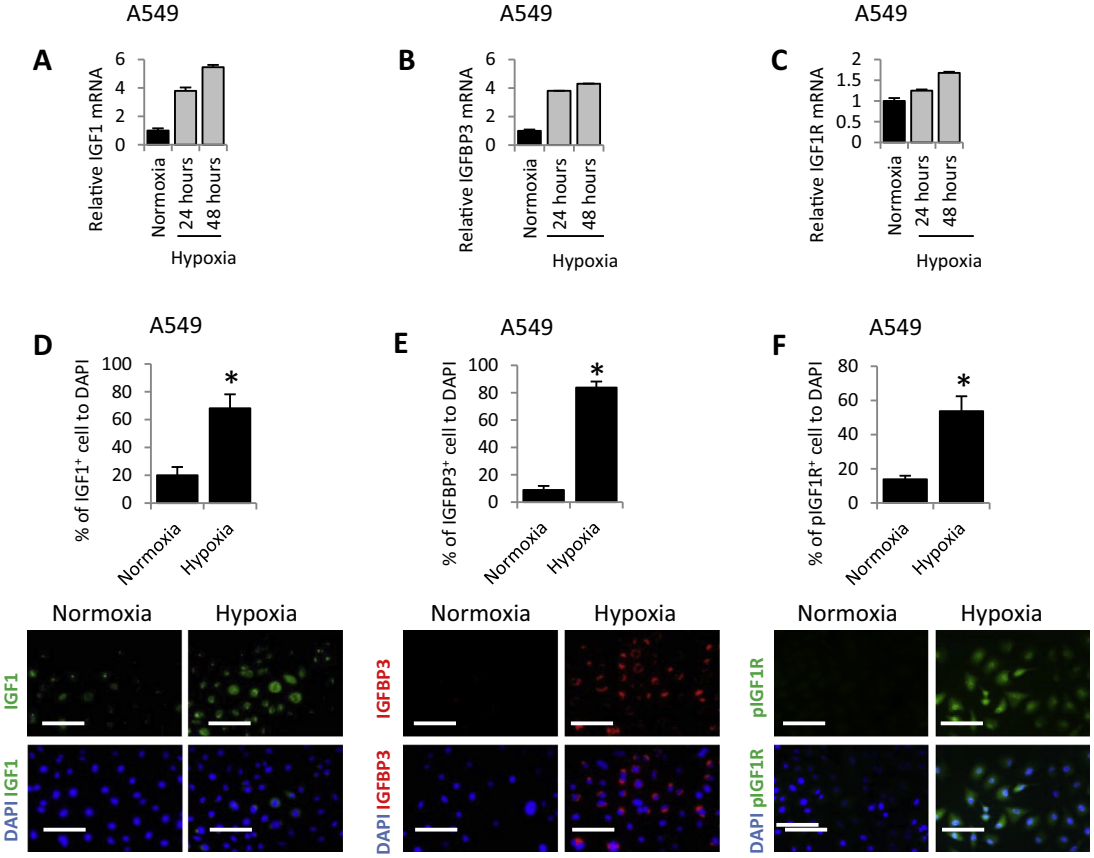

Fig. 2. Hypoxia increased expression of IGFIR-related genes and proteins. Quantitative real-time PCR was performed with primers specific for *IGF1* (A), *IGFBP3* (B), and *IGF1R* (C) in A549 parental and hypoxic cells (24 and 48 h); data were normalized to actin expression. (D–F) A549 cells, grown on Lab-Tek chamber slides exposed to normoxia or hypoxia for 24 h, fixed, and incubated with primary antibodies against IGF1 (D), IGFBP3 (E), or phopho-IGF1R (F) followed by secondary antibodies labeled with Alexa Fluor 488 anti-rabbit IgG (red) or Alexa Fluor 594 anti-mouse IgG (green). Cell nuclei were stained with DAPI (blue). Five images were captured from each group and IGF1$^+$, IGFBP3$^+$, and phopho-IGF1R$^+$ cell numbers were divided by the corresponding DAPI numbers. Data are expressed as the means ± standard deviation. $^*P < 0.05$ indicates a significant difference from control group. Scale bar indicates 200 μM. (For interpretation of the references to color in this figure legend, the reader is referred to the web version of this article.)

utilized the following antibodies: E-cadherin, vimentin, HIF1α (BD Biosciences, Franklin Lakes, NJ, USA), fibronectin (Thermo Scientific, Freemont, CA, USA), IGFBP3 (Santa Cruz Biotechnology, Santa Cruz, CA, USA), phopho-IGF1R (Sigma–Aldrich), and IGF1 antibody (Abcam, Cambridge, England).

2.6. Statistical analysis

Differences between two groups were statistically analyzed using unpaired Student's *t*-test. Differences were considered significant when $P < 0.05$.

3. Results

3.1. Hypoxic A549 and HCC2935 cells underwent morphological changes and increased motility reminiscent of EMT

We first examined the effect of hypoxia on cell morphology of NSCLC cells. Following hypoxia exposure, the morphology of A549 and HCC2935 cells had a markedly different appearance from the parental cell line under light microscopy. Hypoxic A549 cells lost their polarity, and had spindle shape and reduced cell-to-cell contact (Fig. 1A). The same findings were observed in HCC2935 (data not shown). To determine whether hypoxia increased motility of NSCLC cells, we performed scratch wound assay. The image of the scratch taken after 24 h normoxia or hypoxia exposure showed that hypoxic A549 cells filled in the scratch more efficiently than did the normoxic controls (Fig. 1B). These findings suggested that hypoxia induced morphological changes and increased motility and invasiveness that were reminiscent of EMT.

3.2. Exposure to hypoxia induced molecular changes that are associated with EMT

The hallmarks of EMT were reduced epithelial marker such as E-cadherin and increased mesenchymal marker such as vimentin and fibronectin [6]. We analyzed whether the EMT could occur in our hypoxic *in vitro* model using qPCR and immunofluorescence. As shown in Fig. 1C, E-cadherin mRNA expression in A549 cells was reduced after exposure to hypoxia in a time-dependent manner. In contrast, the expression of the mesenchymal markers *fibronectin* and *vimentin* among hypoxic A549 cells increased (Fig. 1C). Furthermore, reduced E-cadherin$^+$ cell population under hypoxia was also evident, as shown in Fig. 1D. Meanwhile, population of fibronectin$^+$ cells (Fig. 1E) as well as of vimentin$^+$ cells (Fig. 1F) were dramatically increased following hypoxia. Similar results were observed in hypoxic HCC2935 cells (Supp. Fig. S1).

It has been reported that EMT could be induced by several factors, including TGFβ. In our hypoxic model, however, *TGFβ* mRNA expression was not upregulated (Supp. Fig. S2). Other known EMT-inducing factors such as epidermal growth factor (*EGF*), hepatocyte growth factor (*HGF*), and *MET* were also not upregulated (data not shown).

3.3. Hypoxia increased expression of IGF1 and IGFBP3 and activated IGF1R in an HIF1α-dependent manner

We next investigated the expression of IGF1R-related factors such as *IGF1*, *IGFBP3*, and *IGF1R* in hypoxic NSCLC cells by qPCR. Hypoxic A549 cells expressed high levels of *IGF1* (Fig. 2A), *IGFBP3* (Fig. 2B), and *IGF1R* (Fig. 2C) in a time-dependent manner. Furthermore, results from immunofluorescence analyses also confirmed increased levels of IGF1 (Fig. 2D) and IGFBP3 protein

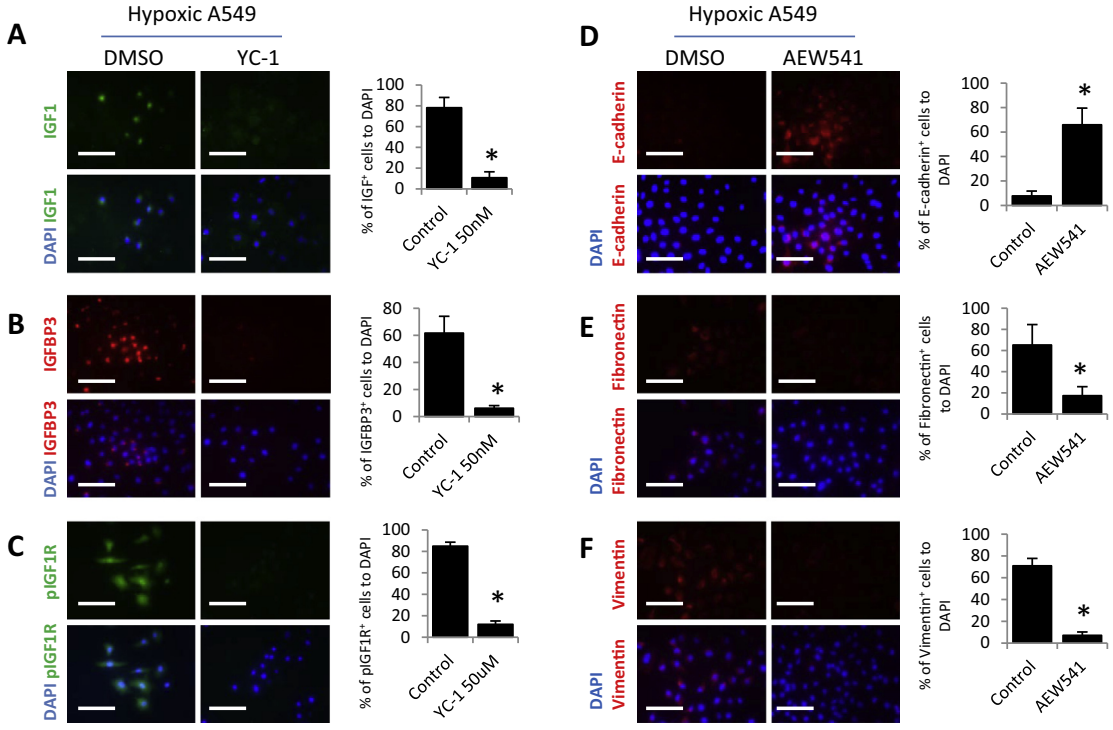

Fig. 3. HIF1α inhibition reduced IGF1R-related factors and inhibition of IGF1R reversed hypoxia-induced EMT. (A–C) A549 cells were exposed to hypoxia and treated with YC-1 (50 μM) or DMSO for 24 h in Lab-Tek chamber slides, followed by immunofluorescence analyses for IGF1 (A), IGFBP3 (B), and phopho-IGF1R (C). IGF1$^+$, IGFBP3$^+$, and phopho-IGF1R$^+$ cell numbers were divided by the corresponding DAPI numbers in five fields in each experiment. (D–F) A549 cells were exposed to hypoxia and treated with AEW541 (0.1 μM) or DMSO for 24 h in Lab-Tek chamber slides followed by immunofluorescence analyses for E-cadherin (D), fibronectin (E), and vimentin (F). E-cadherin$^+$, fibronectin$^+$, and vimentin$^+$ cell numbers were divided by the corresponding DAPI numbers in five fields in each experiment. Data are expressed as the means ± standard deviation. $^*P < 0.05$ indicates a significant difference from the control group. Scale bar indicates 200 μM.

expression (Fig. 2E) in hypoxia-exposed A549 cells. Similar results were obtained in HCC2935 cells (Supp. Fig. S3). Due to the increased expression of IGF1 under hypoxia, we performed further immunofluorescence analyses using a phospho-IG1R antibody in hypoxic A549 and HCC2935 cells (Fig. 2F and Supp. Fig. S3, respectively). We found that hypoxia activated IGF1R in both A549 and HCC2935 cells. In addition, we identified an accumulation of hypoxia-inducible factor 1α (HIF1α) in both hypoxic A549 and HCC2935 cells (Supp. Fig. S4), and therefore investigated whether the upregulation of IGF1 in hypoxia was regulated by HIF1α. We inhibited HIF1α in A549 and HCC2935 cells by treatment with YC-1 and exposed these cells to hypoxia. HIF1α inhibition using YC-1 effectively prevented the accumulation of HIF1α in hypoxic A549 and HCC2935 cells (data not shown). HIF1α inhibition also reduced protein expression of IGF1 (Fig. 3A) and IGFBP3 (Fig. 3B) and prevented activation of IGF1R (Fig. 3C) in A549 cells; similar results were observed in HCC2935 cells (Supp. Fig. S5). These results demonstrated that expression of IGF1 and IGFBP3 was upregulated in NSCLC cells exposed to hypoxia, and that IGF1R was subsequently activated in an HIF1α-dependent manner.

3.4. Inhibition of IGF1R by AEW541 reversed EMT in hypoxic cells

To investigate whether activation of IGF1R was involved in hypoxia-induced EMT, we treated the A549 and HCC2935 cells with AEW541, an IGF1R tyrosine kinase inhibitor, and exposed these cells to hypoxic conditions. AEW541 markedly reduced activation of IGF1R in A549 cells (Supp. Fig. S6A). Furthermore, treatment with AEW541 increased E-cadherin$^+$ cells in hypoxic condition ($P < 0.05$), as shown in Fig. 3D. IGF1R inhibition also reduced fibronectin$^+$ and vimentin$^+$ cell population as measured by immunofluorescence (Fig. 3E and F). Similar results were observed in HCC2935 cells (Supp. Fig. S7). In addition, the motility of hypoxic A549 cells was also reduced with treatment with AEW541 (Supp. Fig. S6B). Taken together, these results indicate that IGF1R activation is involved in hypoxia-induced EMT, and that treatment with IGF1R kinase inhibitor AEW541 would effectively prevent hypoxia-induced EMT in NSCLC cells.

3.5. IGF1 treatment induced EMT in normoxic cells

Finally, we tested whether IGF1R stimulation by its ligand IGF1 could induce EMT in NSCLC cells under normoxic condition. We found that treatment with IGF1 increased the spindle-shaped cell population fraction (Fig. 4A), dramatically reduced E-cadherin expression (Fig. 4B), and increased expression of fibronectin (Fig. 4C) as well as vimentin (Fig. 4D). We further confirmed the activation of phopho-IGF1R by IGF1 stimulation as shown in Fig. 4E. Similar results were observed in HCC2935 cells as well (Supp. Fig. S8). These findings strongly suggested that activation of IGF1R might induce EMT in NSCLC cells.

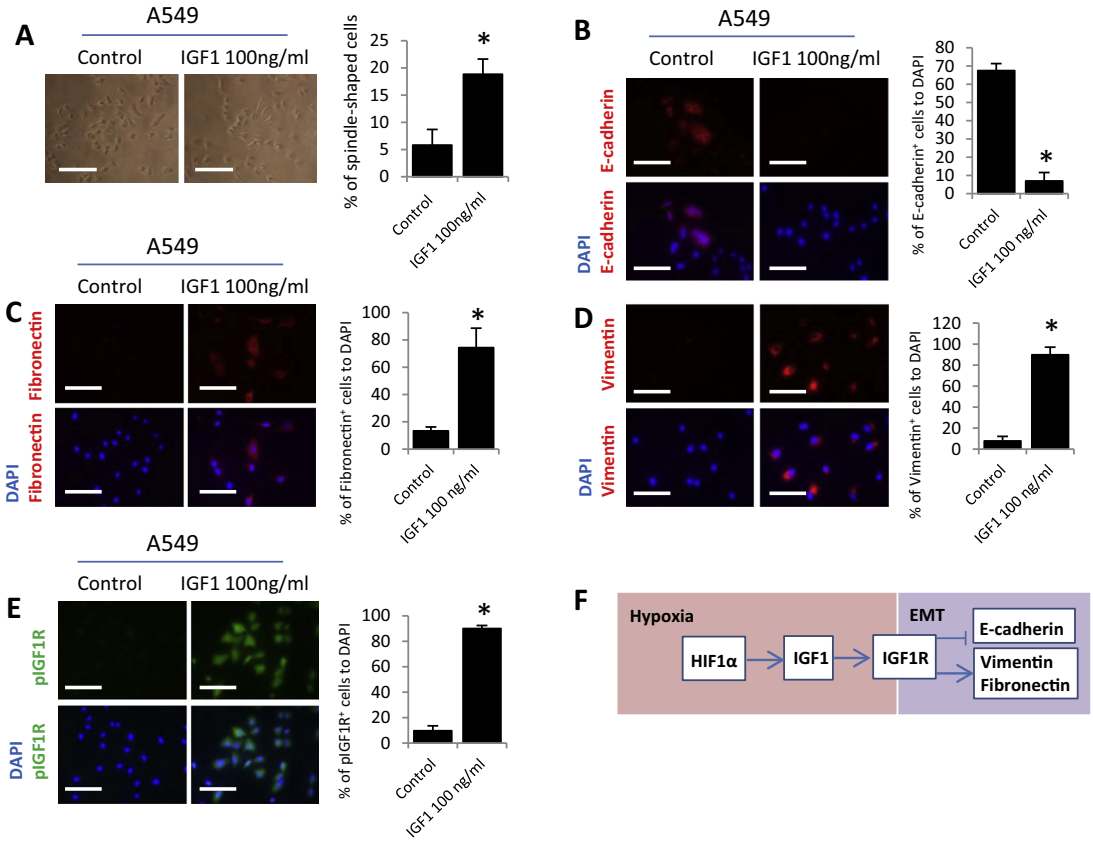

Fig. 4. Stimulation with IGF1 induced EMT in normoxic cells. (A) A549 cells were starved for 24 h followed by stimulation with IGF1 (100 ng/mL) for 24 h and then digital images were taken at 200× magnification by light microscopy. IGF1-stimulated A549 cells were subject to immunofluorescence for E-cadherin (B), fibronectin (C), vimentin (D), and phospho-IGF1R (E) protein expression. Five images were captured from each group and E-cadherin$^+$, vimentin$^+$ and fibronectin$^+$ cell numbers were divided by the corresponding DAPI numbers. Data are expressed as the means ± standard deviation. $^*P < 0.05$ indicates a significant difference from the control group. Scale bar indicates 200 μM. (F) Pathway model: hypoxia induces HIF1α accumulation causing increased expression of IGF1 and subsequent IGF1R activation, resulting in reduced E-cadherin expression and upregulation of the mesenchymal markers vimentin and fibronectin. EMT: epithelial–mesenchymal transition.

4. Discussion

In this study, we demonstrated that hypoxia induced EMT in NSCLC cells and activation of IGF1R was involved in the hypoxia-induced EMT. Polarized and cubical-shaped lung cancer cells were cultured under hypoxic environment, and showed changes in morphology and motility following hypoxia that were reminiscent of EMT. In accordance, qPCR and immunofluorescence showed reduced expression of epithelial- and an increased expression of mesenchymal cell markers in A549 and HCC2935 cells exposed to hypoxia.

Several studies have reported the involvement of TGFβ1 in hypoxia-induced EMT [11]. However in hypoxic A549 and HCC2935 cells, *TGFβ1* expression was not significantly increased in either line (Supp. Fig. S2). These data suggested that hypoxia could induce EMT through an alternative pathway independent from TGFβ1 in our NSCLC model. Therefore, we focused on the possible role of IGF1R pathway. Hypoxic A549 and HCC2935 cells expressed high levels of IGF1R-related factors, such as IGF1, IGF1R, and IGFBP3. In addition, hypoxic condition also induced phosphorylation of IGF1R. Kim et al. [17] showed that IGF1R was activated in hypoxic lung cancer cells. However, there have been no previous reports that investigated the role of IGF1R activation in hypoxia-induced EMT in NSCLC cells.

It has been reported that *IGFBP3*, a hypoxia-inducible gene, regulates a variety of cellular processes including cell proliferation, senescence, apoptosis, and EMT [18]. Our results showed high IGFBP3 expression at both mRNA and protein levels in hypoxic cells. These findings suggest a possible role for IGFBP3 in the hypoxia-induced EMT mediated by IGF1R activation.

Various methods have been developed to interfere with IGF1R signaling, including antisense strategies, monoclonal antibodies, and small-molecule tyrosine kinase inhibitors, some of which are being tested in Phase I or Phase II clinical trials [19]. A systems-based approach has been used to classify IGF1R inhibitors into the following groups: IGF1 antagonists, IGF1R antagonists, IGF1R antibodies, and IGF1R tyrosine kinase inhibitors including AEW541 [20]. Most recent studies have only provided evidence of the use of AEW541 to reduce cell proliferation, induce apoptosis, and reverse cancer treatment resistance in lung cancer. In the present study, we evaluated the possible therapeutic efficacy of AEW541 to reverse hypoxia-induced EMT in NSCLC cells. We demonstrated that IGF1R inhibition rescued E-cadherin expression in hypoxic lung cancer cells. Administration of AEW541 in hypoxic A549 and HCC2935 cells also reduced expression of fibronectin and vimentin, two of the most important mesenchymal markers. These data suggest a potential use of AEW541 to reverse hypoxia-induced EMT phenotypes in NSCLC cells.

To the best of our knowledge, our study is the first to demonstrate a direct linkage between IGF1R activation, hypoxia, and EMT in NSCLC (Fig. 4F). Accumulation of HIF1α upregulates IGF1 expression, resulting in phosphorylation of IGF1R under the hypoxic environment. Activation of IGF1R serves as an alternative pathway to TGFβ1 in promoting hypoxia-induced EMT in NSCLC cells by increasing cell motility, and suppressing the expression of E-cadherin while increasing mesenchymal markers. Our results provide insight into the mechanisms underlying metastasis in NSCLC, and support the proposition that IGF1R inhibition might be considered as one of the methods for future utilization to prevent cancer progression and metastasis.

Conflict of interest

The authors report no conflicts of interest for this work.

Acknowledgments

This study was supported by Grants-in-Aid for Scientific Research No. 23591906 (Fumiyuki Takahashi) and by Post-graduate Scholarship, No. 91006006265 (Fariz Nurwidya) from the Ministry of Education, Culture, Sports, Science, and Technology of Japan. We received important advice and expertise from Ms. Takako Ikegami and Ms. Tomomi Ikeda, Laboratory of Molecular and Biochemical Research, Research Support Center, Juntendo University Graduate School of Medicine; and from Dr. Yuko Kojima, Mr. Noriyoshi Sueyoshi, and Dr. Katsumi Miyahara, Laboratory of Biomedical Imaging Research, Biomedical Research Center.

Appendix A. Supplementary data

Supplementary data associated with this article can be found, in the online version, at http://dx.doi.org/10.1016/j.bbrc.2014.11.014.

References

[1] M. Pollak, Insulin and insulin-like growth factor signalling in neoplasia, Nat. Rev. Cancer 8 (2008) 915–928.
[2] J.A. Valdes, S. Flores, E.N. Fuentes, C. Osorio-Fuentealba, E. Jaimovich, A. Molina, IGF-1 induces IP3-dependent calcium signal involved in the regulation of myostatin gene expression mediated by NFAT during myoblast differentiation, J. Cell. Physiol. 228 (2013) 1452–1463.
[3] R. Siegel, J. Ma, Z. Zou, A. Jemal, Cancer statistics, 2014, CA Cancer J. Clin. 64 (2014) 9–29.
[4] M. Iwatsuki, K. Mimori, T. Yokobori, H. Ishi, T. Beppu, S. Nakamori, H. Baba, M. Mori, Epithelial–mesenchymal transition in cancer development and its clinical significance, Cancer Sci. 101 (2010) 293–299.
[5] L. Wan, K. Pantel, Y. Kang, Tumor metastasis: moving new biological insights into the clinic, Nat. Med. 19 (2013) 1450–1464.
[6] A. Singh, J. Settleman, EMT, cancer stem cells and drug resistance: an emerging axis of evil in the war on cancer, Oncogene 29 (2010) 4741–4751.
[7] J.P. Thiery, H. Acloque, R.Y. Huang, M.A. Nieto, Epithelial–mesenchymal transitions in development and disease, Cell 139 (2009) 871–890.
[8] L. Jiang, L. Xiao, H. Sugiura, X. Huang, A. Ali, O.M. Kuro, R.J. Deberardinis, D.A. Boothman, Metabolic reprogramming during TGFbeta1-induced epithelial-to-mesenchymal transition, Oncogene (2014).
[9] C.W. Li, W. Xia, L. Huo, S.O. Lim, Y. Wu, J.L. Hsu, C.H. Chao, H. Yamaguchi, N.K. Yang, Q. Ding, Y. Wang, Y.J. Lai, A.M. LaBaff, T.J. Wu, B.R. Lin, M.H. Yang, G.N. Hortobagyi, M.C. Hung, Epithelial–mesenchymal transition induced by TNF-alpha requires NF-kappaB-mediated transcriptional upregulation of Twist1, Cancer Res. 72 (2012) 1290–1300.
[10] G. Zhou, L.A. Dada, M. Wu, A. Kelly, H. Trejo, Q. Zhou, J. Varga, J.I. Sznajder, Hypoxia-induced alveolar epithelial–mesenchymal transition requires mitochondrial ROS and hypoxia-inducible factor 1, Am. J. Physiol. Lung Cell. Mol. Physiol. 297 (2009) L1120–L1130.
[11] J. Matsuoka, M. Yashiro, Y. Doi, Y. Fuyuhiro, Y. Kato, O. Shinto, S. Noda, S. Kashiwagi, N. Aomatsu, T. Hirakawa, T. Hasegawa, K. Shimizu, T. Shimizu, A. Miwa, N. Yamada, T. Sawada, K. Hirakawa, Hypoxia stimulates the EMT of gastric cancer cells through autocrine TGFbeta signaling, PLoS One 8 (2013) e62310.
[12] L. Zhang, G. Huang, X. Li, Y. Zhang, Y. Jiang, J. Shen, J. Liu, Q. Wang, J. Zhu, X. Feng, J. Dong, C. Qian, Hypoxia induces epithelial–mesenchymal transition via activation of SNAI1 by hypoxia-inducible factor-1alpha in hepatocellular carcinoma, BMC Cancer 13 (2013) 108.
[13] J. Huang, X. Yao, J. Zhang, B. Dong, Q. Chen, W. Xue, D. Liu, Y. Huang, Hypoxia-induced downregulation of miR-30c promotes epithelial–mesenchymal transition in human renal cell carcinoma, Cancer Sci. 104 (2013) 1609–1617.
[14] A.V. Salnikov, L. Liu, M. Platen, J. Gladkich, O. Salnikova, E. Ryschich, J. Mattern, G. Moldenhauer, J. Werner, P. Schemmer, M.W. Buchler, I. Herr, Hypoxia induces EMT in low and highly aggressive pancreatic tumor cells but only cells with cancer stem cell characteristics acquire pronounced migratory potential, PLoS One 7 (2012) e46391.
[15] K. Hongo, N.H. Tsuno, K. Kawai, K. Sasaki, M. Kaneko, M. Hiyoshi, K. Murono, N. Tada, T. Nirei, E. Sunami, K. Takahashi, H. Nagawa, J. Kitayama, T. Watanabe, Hypoxia enhances colon cancer migration and invasion through promotion of epithelial–mesenchymal transition, J. Surg. Res. 182 (2013) 75–84.
[16] X. Zhao, W. Dou, L. He, S. Liang, J. Tie, C. Liu, T. Li, Y. Lu, P. Mo, Y. Shi, K. Wu, Y. Nie, D. Fan, MicroRNA-7 functions as an anti-metastatic microRNA in gastric cancer by targeting insulin-like growth factor-1 receptor, Oncogene 32 (2013) 1363–1372.
[17] T.R. Kim, E.W. Cho, S.G. Paik, I.G. Kim, Hypoxia-induced SM22alpha in A549 cells activates the IGF1R/PI3K/Akt pathway, conferring cellular resistance against chemo- and radiation therapy, FEBS Lett. 586 (2012) 303–309.

[18] M. Natsuizaka, H. Kinugasa, S. Kagawa, K.A. Whelan, S. Naganuma, H. Subramanian, S. Chang, K.J. Nakagawa, N.L. Rustgi, Y. Kita, S. Natsugoe, D. Basu, P.A. Gimotty, A.J. Klein-Szanto, J.A. Diehl, H. Nakagawa, IGFBP3 promotes esophageal cancer growth by suppressing oxidative stress in hypoxic tumor microenvironment, Am. J. Cancer Res. 4 (2014) 29–41.

[19] S.F. Isebaert, J.V. Swinnen, W.H. McBride, K.M. Haustermans, Insulin-like growth factor-type 1 receptor inhibitor NVP-AEW541 enhances radiosensitivity of PTEN wild-type but not PTEN-deficient human prostate cancer cells, Int. J. Radiat. Oncol. Biol. Phys. 81 (2011) 239–247.

[20] M. Hewish, I. Chau, D. Cunningham, Insulin-like growth factor 1 receptor targeted therapeutics: novel compounds and novel treatment strategies for cancer medicine, Recent Pat. Anticancer Drug Discov. 4 (2009) 54–72.